sensors

MDPI

Article

Fano Resonance Based on Metal-Insulator-Metal Waveguide-Coupled Double Rectangular Cavities for Plasmonic Nanosensors

Zhidong Zhang [1,2], Liang Luo [1,2], Chenyang Xue [1,2], Wendong Zhang [1,2] and Shubin Yan [1,2,*]

1 Science and Technology on Electronic Test & Measurement Laboratory, North University of China, No. 3 Xueyuan Road, Taiyuan 030051, China; zdzhang@nuc.edu.cn (Z.Z.); 15135165573@163.com (L.L.); xuechenyang@nuc.edu.cn (C.X.); wdzhang@nuc.edu.cn (W.Z.)

2 Key Laboratory of Instrumentation Science & Dynamic Measurement, Ministry of Eduction, North University of China, No. 3 Xueyuan Road, Taiyuan 030051, China

* Correspondence: shubin_yan@nuc.edu.cn; Tel.: +86-351-392-0398

Academic Editor: Stephane Evoy
Received: 17 February 2016; Accepted: 29 April 2016; Published: 5 May 2016

Abstract: A refractive index sensor based on metal-insulator-metal (MIM) waveguides coupled double rectangular cavities is proposed and investigated numerically using the finite element method (FEM). The transmission properties and refractive index sensitivity of various configurations of the sensor are systematically investigated. An asymmetric Fano resonance lineshape is observed in the transmission spectra of the sensor, which is induced by the interference between a broad resonance mode in one rectangular and a narrow one in the other. The effect of various structural parameters on the Fano resonance and the refractive index sensitivity of the system based on Fano resonance is investigated. The proposed plasmonic refractive index sensor shows a maximum sensitivity of 596 nm/RIU.

Keywords: surface plasmon polaritons; metal-insulator-metal waveguide; Fano resonance; refractive index sensor; finite element method

1. Introduction

In the direction perpendicular to the metal-insulator interface, the surface plasmon polaritons (SPPs) energy shows an exponential decay function [1,2]. As a result, the SPPs are strongly confined to near the metal-insulator interface, and can overcome the traditional optical diffraction limitation [3–5]. The strong SPPs at metal-dielectric interfaces can enhance molecular signals [6,7], making it useful in high-sensitivity sensors such as temperature sensors [8], biosensors and chemical sensors [9–11]. In addition, SPPs are regarded as a promising information carrier for next-generation ultrahigh-density photonic integrated circuits [12].

Metal-insulator-metal (MIM) waveguide-coupled resonators have attracted considerable research interest because of their easy on-chip integration and deep-subwavelength confinement of light [13,14]. Many photonic devices based on MIM waveguides have been designed and investigated, such as filters [15], wavelength division multiplexers [16], and high-sensitivity plasmonic sensors [17]. Plasmonic sensors based on MIM waveguides [13,14,18] have received considerable research interest because of the need for ultrahigh-sensitivity biochemical sensors [19,20]. Plasmonic devices based on Fano resonance exhibit great sensitivity and large figure of merit (FOM) [14,21]; these properties make Fano resonance appealing for use in sensors, lasing, switching, nonlinear and slow-light devices [18,22–24]. The plasmonic refractive index sensor with diverse structure are investigated, such as MIM waveguide coupled only resonator [25–27] and MIM waveguide coupled composite resonator [28,29]. Although the plasmonic sensor own the advantage of small size, and ease to

integration, but its sensitivity is not as high as that of fiber sensor (30,100 nm/RIU) [25]. Therefore, how to optimize the plasmonic refractive index structure design to improve the sensitivity is a key issue for designing plasmonic sensor. Fano resonance is extremely sensitive to changes in the refractive index because it is a weak interference phenomenon that has unique line shape [30,31], which provides a very promising pathway to achieve ultrahigh sensitivity sensor. Fano resonances can be obtained from the interaction between the narrow discrete modes and broad continuous modes inside a subwavelength cavity [24].

In this paper, we design a plasmonic refractive index nanosensor based on a MIM waveguide-coupled double rectangular cavities, which is composed of two MIM waveguides and double rectangular cavities. Compared with other sensors, SPPs sensors have an inherent advantage to achieve high integration. The transmission spectrum and magnetic field distributions of the nanosensor are simulated using the finite element method (FEM) with a perfectly matched layer (PML) absorbing boundary condition. The effects of the structural parameters of the MIM waveguide-coupled double rectangular cavity on the propagation properties of the nanosensor are studied. The proposed structure can be easily integrated with various photonic devices and chips.

2. Structural and Analytical Method

Considering that three-dimensional (3D) model simulation requires too many computer resources and the limitations of our computer workstation, the two-dimensional (2D) plasmonic waveguide coupled resonator system was investigated by the FEM in this paper. The working principle of the 2D model as similar to that of the real 3D model, because in real photonic devices if the depth of the metal layer is large enough (*i.e.*, the third dimension much larger than the light wavelength), then the properties of the 3D model can be approximated by a 2D model. Figure 1 illustrates the geometry of the designed 2D MIM waveguide-coupled double rectangular cavity, which consists of two straight MIM waveguides with one end sealed and double rectangular cavities with a parallel arrangement. One rectangular cavity behaves as the active cavity, and the other rectangular cavity as the passive cavity. To ensure fundamental transverse magnetic (TM_0) mode propagation in the MIM waveguide, the insulator layer width of the MIM waveguide was fixed at w = 50 nm [32]. The input port (P_1) and output port (P_2) are located in the left and the right end of the MIM waveguide, respectively. The coupling distance between the MIM waveguide and rectangular cavity is g_1 (5 nm) and the gap between the double rectangular cavities is g_2. The widths of the left and right rectangular cavities are d_1 and d_2, respectively. The height of the double rectangular cavities is h. The refractive index of the dielectric layer (white) in the MIM waveguide and rectangular cavity is denoted as n.

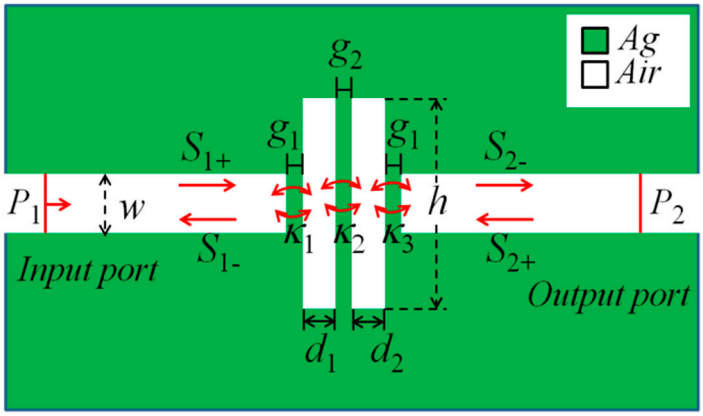

Figure 1. Schematics of the proposed MIM waveguide-coupled double rectangular cavities.

The propagation properties of the MIM waveguide-coupled double rectangular cavities were simulated by the FEM. PMLs were set at the up and bottom boundaries of the structure. The

frequency-dependent complex relative permittivity $\varepsilon(\omega)$ of silver is characterized by the modified Debye-Drude dispersion model [33]:

$$\varepsilon(\omega) = \varepsilon_\infty + (\varepsilon_s - \varepsilon_\infty)/(1 + i\omega\tau) + \sigma/i\omega\varepsilon_0 \quad (1)$$

where the infinite permittivity ε_∞ = 3.8344, static permittivity ε_s = −9530.5, relaxation time $\tau = 7.35 \times 10^{-15}$, and conductivity σ =1.1486 × 10^7 s/m.

For MIM waveguide coupling resonator, the resonance wavelength can be determined by [34,35]:

$$\lambda_m = \frac{2\mathrm{Re}(n_{eff})L}{m - \psi_r/\pi}(m = 1, 2, \cdots) \quad (2)$$

where L is the perimeter of the cavities, positive integer m is the number of antinodes of the standing SPP wave, and ψ_r is the phase shift of the beam reflected at one end of the cavity. Re(n_{eff}) is the real part of the effective refractive index in MIM waveguide, which can be obtained by solving the dispersion relation of the TM_0 mode in a MIM waveguide.

The TM_0 model equation in the MIM waveguide is [15,32]:

$$tanh\ (kd) = -2kp\alpha_c/\left(k^2 + p^2{\alpha_c}^2\right) \quad (3)$$

where k and d are the wave vector in the waveguide and the width of the MIM waveguide, respectively. The parameters p and α_c in Equation (3) are defined as $p = \varepsilon_{in}/\varepsilon_m$ and $\alpha_c = [{k_0}^2\ (\varepsilon_{in} - \varepsilon_m) + \kappa]^{1/2}$. ε_{in} and ε_m are the dielectric constants of the insulator and metal, respectively. The wave vector in free space $k_0 = 2\pi/\lambda_0$. Therefore, k can be solved from Equation (3) using the iterative method. Thus, the effective index neff of the MIM waveguide can be expressed as $\mathrm{Re}(n_{eff}) = [\varepsilon_m + (k/k_0)^2]^{1/2}$. The wavelength of SPPs λ_{spp} can be obtained from $\lambda_{spp} = \lambda_0/\mathrm{Re}(n_{eff})$. P_1 is defined as the input port, and P_2 is the output port. The transmission of the MIM waveguide coupling cavity is determined as $T = (S_{21})^2$, where S_{21} is the transmission coefficient from port 1 to port 2. In addition, FOM was used to evaluate the sensitivity of the refractive index sensor. FOM is defined as $(\delta\lambda/\delta n)/\mathrm{FWHM}$, where $\delta\lambda$ is the wavelength change corresponding to the refractive index change δn, and FWHM is the full width at half-maximum of the resonance peak.

For the MIM waveguide coupled double rectangular cavities system, the temporal coupled mode theory (CMT) [36,37] is utilized to analyze in detail the Fano resonance in this paper. The amplitudes of the SPPs wave of the cavity are denoted by $S_i \pm$ (i = 1, 2, and 3), and the subscripts $\pm$ of $S_i\pm$ denote the input and output from the rectangular cavity (as shown in Figure 1), respectively. When an optical wave with a frequency ω is launched only from the input port of the MIM waveguide (S_{2+} = 0), the time evolution amplitude $A_i \pm$ (i = 1,2, and 3) of the cavity can be expressed as [38]:

$$\frac{dA_1}{dt} = (j\omega_1 - 1/\tau_1 - 1/\tau_2)\,A_1 + \kappa_1 S_{1+} + \kappa_2 A_2 \quad (4)$$

$$\frac{dA_2}{dt} = (j\omega_2 - 1/\tau_2 - 1/\tau_3)\,A_2 + \kappa_3 S_{2+} + \kappa_2 A_1 \quad (5)$$

Here κ_1 and κ_3 are the coupling coefficients between the MIM waveguide and rectangular cavities, and κ_2 is the coupling coefficient between the left rectangular cavity and right rectangular cavity. Then we can write $1/\tau_1 = {\kappa_1}^2$ and $1/\tau_3 = {\kappa_3}^2$ as the corresponding decay rates from the cavity to MIM waveguide, and $1/\tau_2 = {\kappa_2}^2$ is the decay rate from the left cavity to right cavity (or from right cavity to left cavity), ω_1 and ω_2 are the resonance frequency of the left and the right resonator, respectively. j is the imaginary unit ($j^2 = -1$). According to energy conservation. The amplitude of the input and the output waves in coupled waveguide should satisfy the following relationships:

$$S_{2-} = j\sqrt{\kappa_3}A_2 \quad (6)$$

$$S_{1-} = S_{1+} + j\sqrt{\kappa_1}A_1 \tag{7}$$

Therefore, the transmittance of the system can be solved from Equations (4)–(7) and can be expressed as:

$$T = \left|\frac{S_{2-}}{S_{1+}}\right|^2 = \left|\frac{\kappa_1\kappa_2\kappa_3}{[j(\omega-\omega_1)+1/\tau_1+1/\tau_2][j(\omega-\omega_2)+1/\tau_2+1/\tau_3]-\kappa_2^2}\right|^2 \tag{8}$$

When $\kappa_2 = 0$, T = 0. But $\kappa_2 \neq 0$, the coupling between double rectangular cavities significantly perturbs the wave transmitted from the left waveguide to right waveguide, which result in a complex interference phenomena, and makes the system exhibit a Fano line shape.

3. Results and Discussion

Figure 2 shows the transmission spectrum of the MIM waveguide-coupled double rectangular cavities with $d_1 = d_2 = 10$ nm, $h = 100$ nm, $g_1 = g_2 = 5$ nm and $n = 1$. A resonance peak with asymmetric line shape is observed. The slope of the left shoulder of the resonance peak is obviously larger than that of the right shoulder, which is a typical Fano profile with one maximum and one minimum. The transmittance is near to 0 at the transmission dip ($\lambda = 580$ nm). The dip is regarded as a superradiative mode but the peak as a nonoradiative mode.

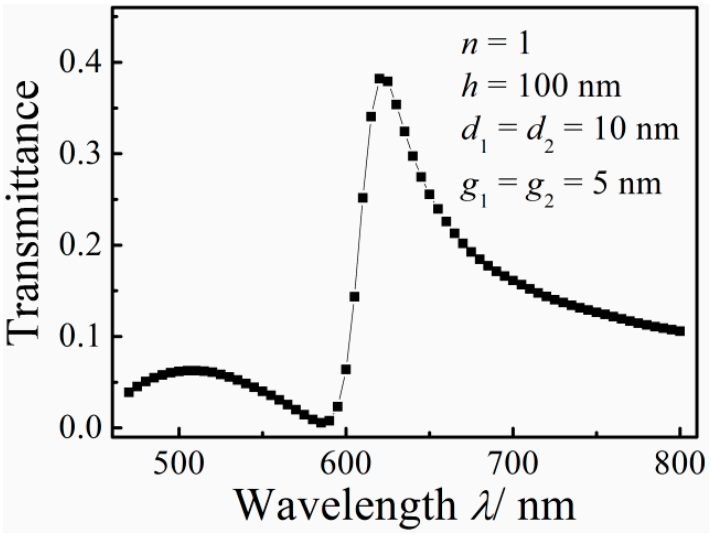

Figure 2. Transmission spectrum of the MIM waveguide-coupled double rectangular cavities.

Figure 3a,b display the normalized magnetic field H_z distributions for the transmission dip ($\lambda_{dip} = 580$ nm) and transmission peak ($\lambda_{peak} = 620$ nm) of the MIM waveguide-coupled double rectangular cavities, respectively. For the superradiative mode ($\lambda_{dip} = 580$ nm), the H_z field distributions show that there is in-phase between the double rectangular cavities. A very weaken coupling occur between double rectangular cavities, and have no SPPs coupled into the right MIM waveguide, which agrees well with the result ($\kappa_2 = 0$, $T = 0$) from Equation (8). For the nonradiative mode ($\lambda_{peak} = 620$ nm), the H_z fields distribution show that there is anti-phase between double rectangular cavities. The superradiative mode is excited by the SPPs from input waveguide, the nonradiative mode cannot. However, it can be excited by the near-field associated with the superradiative mode. Fano resonances arise from the interaction between the superradiative (discrete state) mode and the nonradiative mode (continuum state).

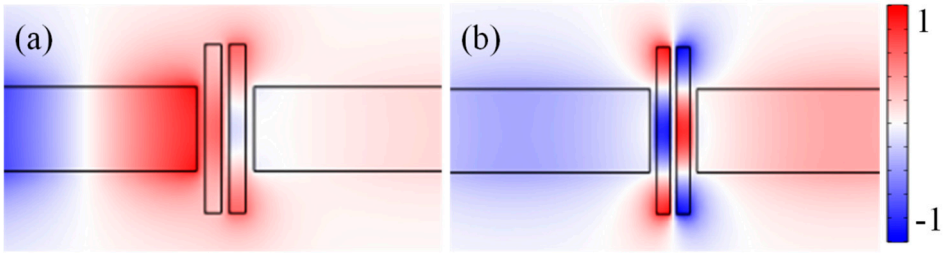

Figure 3. Steady state magnetic field H_z distributions for the (**a**) transmission dip (580 nm); and (**b**) transmission peak (620 nm) of the MIM waveguide-coupled double rectangular cavities.

To investigate the sensitivity of the Fano resonance of the proposed nanosensor to n, dielectrics with different n were filled in the MIM waveguides and double rectangular cavities. Figure 4a depicts the transmission spectra of the MIM waveguide-coupled double rectangular cavities with n of 1–1.05 RIU in increments of 0.01 RIU; others structural parameters g_1, d, h, and g_2 were fixed at 5, 10, 100, and 5 nm, respectively. With increasing n, Re(n_{eff}) increased. The Fano resonance peak showed a red shift as n increased. These Fano resonance peak red shifts can also be explained using Equation (2). The transmission spectra reveal that the transmittance of the Fano resonance peak increased with increasing n. Figure 4b shows the shift of the Fano resonance peak as a function of δn. The solid curves are the linear fittings. The sensitivity $\delta\lambda/\delta n$ of the refractive index sensor is 495 nm/RIU according to Figure 4b, and its FOM is 7.5.

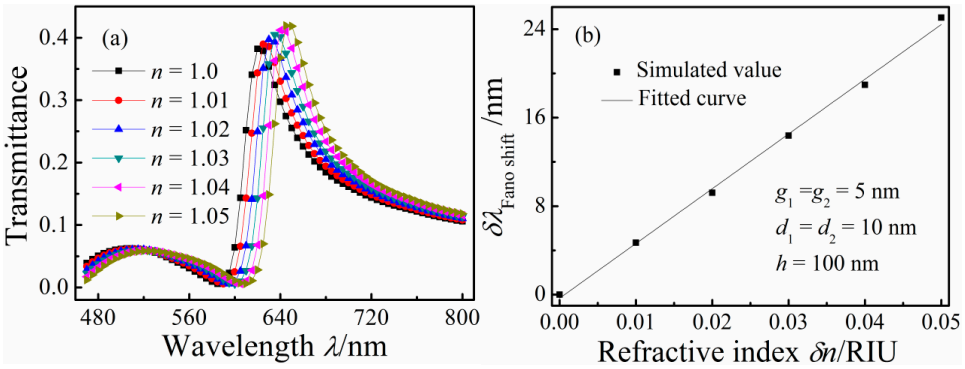

Figure 4. (**a**) Transmission spectra for different refractive index n; and (**b**) the shift of the Fano resonance peak as a function of the refractive index change δn.

To study the effect of the double rectangular cavities widths on the Fano resonance of the MIM waveguide-coupled double rectangular cavities, d_1 and d_2 were increased synchronously from $d_1 = d_2 = 10$ nm to $d_1 = d_2 = 20$ nm with fixed $h = 100$ nm, $g = g_1 = 5$ nm, and $n = 1$ RIU. The transmission spectra of the MIM waveguides coupled different double rectangular cavities widths for $d_1 = d_2 = 10$, 12, 14, 16, 18, and 20 nm are presented in Figure 5a. With increasing double rectangular cavities widths ($d_1 = d_2$), the Fano resonance of the system blue shifts obviously. This can be explained by the increase of d_1 and d_2 decreasing Re(n_{eff}), and the blue shift of the Fano resonance peak is also predicted by above Equation (2). Figure 5b shows the shift of the Fano resonance peak ($d_1 = d_2 = 12$, 16, and 20 nm) as a function δn. The solid curves are the linear fittings. The sensitivity $\delta\lambda/\delta n$ of the nanosensor with $d_1 = d_2 = 12$ nm is equal to that of the configuration with $d_1 = d_2 = 16$ nm, with a value of 498.2 nm/RIU. Compared with the nanosensor with $d_1 = d_2 = 12$ and 16 nm, $\delta\lambda/\delta n$ for the configuration with $d_1 = d_2 = 20$ nm decreases obviously to 335.2 nm/RIU. As shown in Figure 5c, the Fano resonance peak change as the widths ($d_1 = d_2$) is an exponential decay function from the $d_1 = d_2 = 10$ nm to $d_1 = d_2 = 16$ nm, but it is linear function from $d_1 = d_2 =16$ nm to $d_1 = d_2 = 20$ nm. The

point (d_1 = d_2 = 16 nm) is a inflection point of the function of Fano peak as the d_1 (d_2), so an abrupt change is observed from d_1 = d_2 = 16 nm to d_1 = d_2 = 20 nm.

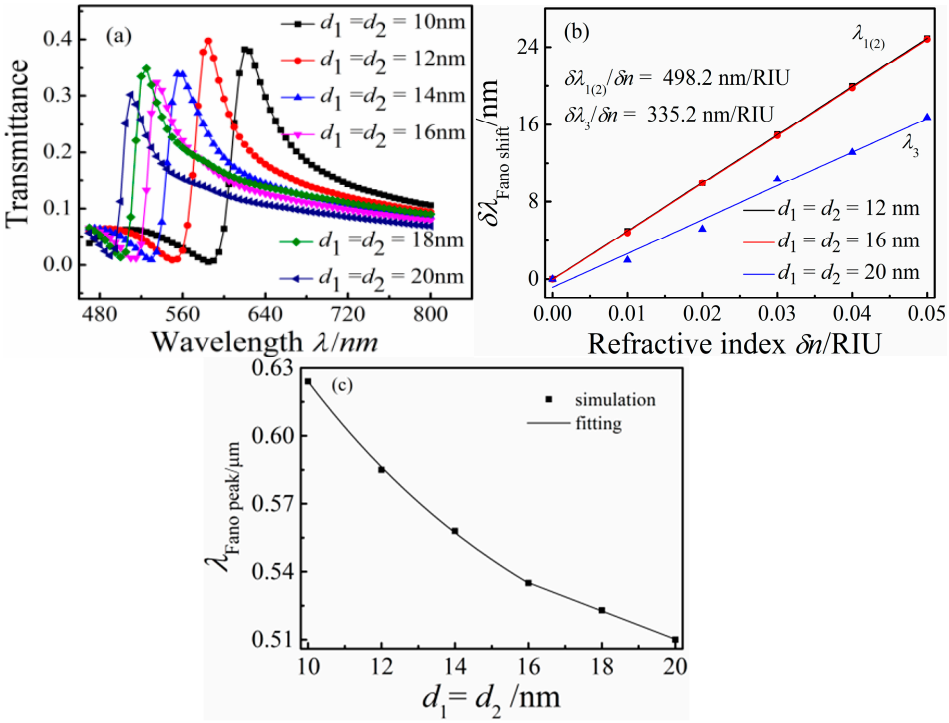

Figure 5. (**a**) Transmission spectra for different rectangular cavity widths d_1(d_2); (**b**) the shift of the Fano resonance peak as a function of the refractive index change δn; and (**c**) the Fano resonance peak as a function of the rectangular cavity widths change d_1(d_2).

Figure 6a shows that the transmission spectra when d_1 is increased from 10 to 20 nm in 2 nm increments with fixed d_2 = 10 nm, h = 100 nm, g = g_1 = 5 nm, and n = 1 RIU. With increasing d_1, the blue shift and the transmittance of the Fano resonance peak decreased slightly. The increase of d_1 caused Re(n_{eff}) to decrease in the rectangular cavity. Figure 6b shows the shift of the Fano resonance peak $\delta\lambda_{\text{Fano shift}}$ as a function of δn, from which we calculated that $\delta\lambda/\delta n$ is 505.6 nm/RIU for this configuration. In addition, we fixed d_1 to investigate the effect of varying d_2 on the transmission spectra. Figure 6c displays the transmission spectra for systems with d_2 = 10, 12, 14, 16, 18, and 20 nm with fixed d_1 = 10 nm. With increasing d_2, the Fano resonance peak blue shifts and its transmittance decreases slightly. Figure 6d presents $\delta\lambda_{\text{Fano shift}}$ plotted as a function of δn for the configurations with different d_2; $\delta\lambda/\delta n$ determined from this plot is 502 nm/RIU.

The simulation indicate that the Fano resonance peak as the changing of the refractive index is linear function, and they parallel to each other nearly for different d_1 or d_2, namely they have same slope. So the refractive index sensitivity $\delta\lambda/\delta n$ curves overlapped each other. To investigate how h affects the Fano resonance of the MIM waveguide-coupled double rectangular cavities, transmission spectra for different height h of 80, 90, 100, 110, and 120 nm with g = g_1 = 5 nm, d = 10 nm, and n = 1 RIU were calculated, and are plotted in Figure 7a. With increasing h, the Fano resonance peak red-shifted linearly because the SPPs pathway in the rectangular cavity lengthened, and its transmittance increased. Figure 7b illustrates the shift of the Fano resonance peak as a function of δn for h = 70, 100, 120 nm. The solid curve is the linear fitting. With increasing h, $\delta\lambda/\delta n$ increased. For h = 70, 100, and 120 nm, $\delta\lambda/\delta n$ are 331, 498, and 596 nm/RIU.

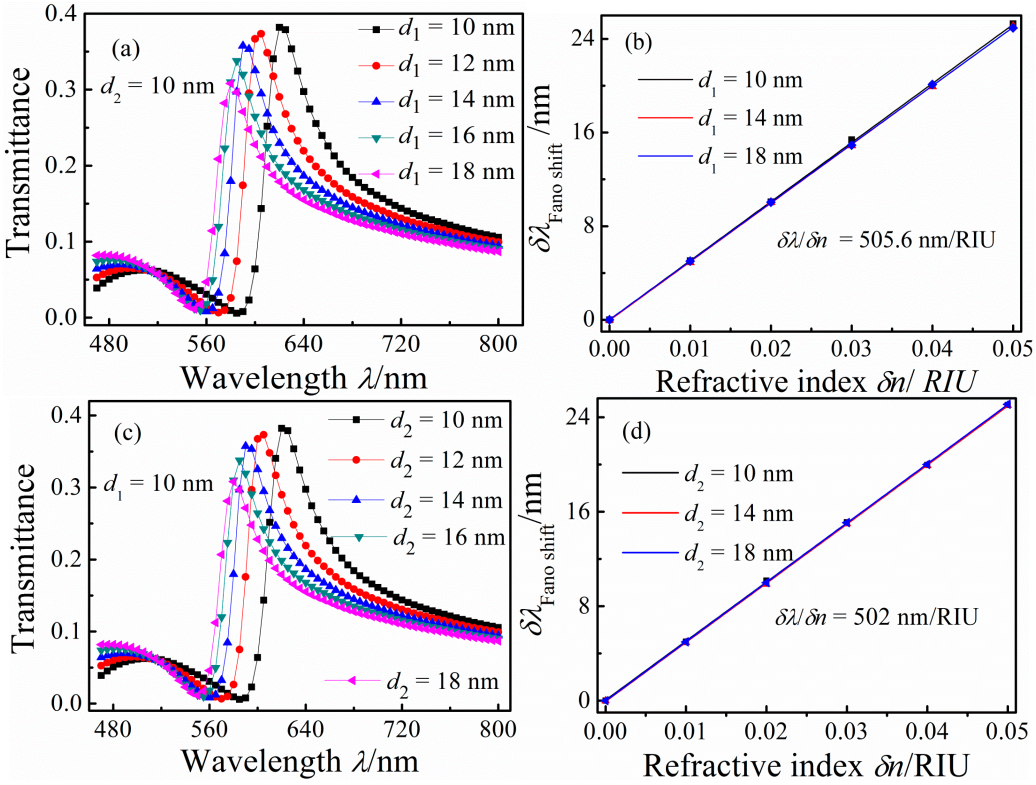

Figure 6. (**a**,**c**) Transmission spectra for different rectangular cavities width d_1 (**a**) and d_2 (**c**); respectively; (**b**,**d**) the shift of the Fano resonance peak as a function of δn with different rectangular cavities width d_1 (**b**) and d_2 (**d**), respectively.

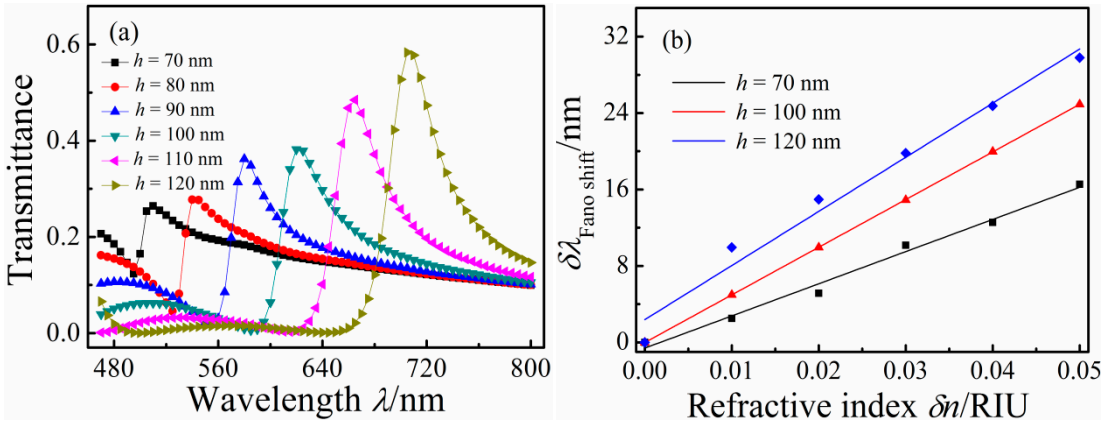

Figure 7. (**a**) Transmission spectra; and (**b**) Fano resonance wavelengths of MIM waveguides-coupled double rectangular cavities with different double rectangular cavities heights h.

4. Conclusions

The transmission properties of MIM waveguide-coupled double rectangular cavities were studied using the FEM. A Fano resonance peak was observed in transmission spectra, and it depended on the mode coupling between the double rectangular cavities. Upon increasing the width of the double rectangular cavities simultaneously, the Fano resonance peak blue shifted and its transmittance decreased, and the sensitivity decreased. Upon increasing the width of one rectangular cavity, the Fano resonance peak blue shifted and the sensitivity did not change. The Fano resonance peak exhibited an obvious red shift and its transmittance increased with increasing height of the double rectangular

cavities; the sensitivity also increased obviously. The refractive index sensitivity (596 nm/RIU) of the MIM waveguide coupled double rectangular cavities is higher than the previously [27]. The sensitivity of the proposed sensor based on waveguide coupled resonance is smaller than that of the conventional SPR sensor based on Kretschmann geometry [39], but the former is easier to integrate with various photonic devices and chips than the latter.

Acknowledgments: This work was supported by the National Natural Science Foundation of China (Grant No. 61275166), the Fund Program for the Scientific Activities of Selected Returned Overseas Professionals in Shanxi Province, the Science Foundation of North University of China (Grant No. 110246), Program for the Top Young and Middle-aged Innovative Talents of Higher Learning Institutions of Shanxi, and the North University of China Science Fund for Distinguished Young Scholars.

Author Contributions: Zhi-Dong Zhang analyzed the data and wrote the paper; Zhi-Dong Zhang, Liang Luo and Shu-Bin Yan conceived and designed the simulations; Liang Luo performed the simulations; Shu-Bin Yan revised the paper; Chen-Yang Xue and Wen-Dong Zhang contributed analysis tools.

Conflicts of Interest: The authors declare no conflict of interest.

Abbreviations

The following abbreviations are used in this manuscript:

SPPs	Surface plsmon polartions
MIM	Metal-insulator-metal
FEM	Finite element method
FOM	Figure of merit
PML	Perfectly matched layer
3D	Three-dimensional
2D	Two-dimensional
CMT	Coupled mode theory
TM_0	Fundamental transverse magnetic
FWHM	Full width at half-maximum

References

1. Barnes, W.L.; Dereux, A.; Ebbesen, T.W. Surface plasmon subwavelength optics. *Nature* **2003**, *424*, 824–830. [CrossRef] [PubMed]
2. Zayats, A.V.; Smolyaninov, I.I.; Maradudin, A.A. Nano-optics of surface plasmon polaritons. *Phys. Rep.* **2005**, *408*, 131–314. [CrossRef]
3. Yin, Y.; Qiu, T.; Li, J.; Chu, P.K. Plasmonic nano-lasers. *Nano Energy* **2012**, *1*, 25–41. [CrossRef]
4. Zafar, R.; Salim, M. Achievement of large normalized delay bandwidth product by exciting electromagnetic-induced transparency in plasmonic waveguide. *IEEE J. Quantum Electron.* **2015**, *51*, 7200306–7200312. [CrossRef]
5. Zhang, Z.D.; Wang, H.Y.; Zhang, Z.Y. Fano resonance in a gear-shaped nanocavity of the metal-insulator-metal waveguide. *Plasmonics* **2012**, *8*, 797–801. [CrossRef]
6. Hakala, T.K.; Toppari, J.J.; Kuzyk, A.; Pettersson, M.; Tikkanen, H.; Kunttu, H.; Törmä, P. Vacuum Rabi splitting and strong-coupling dynamics for surface-plasmon polaritons and rhodamine 6G molecules. *Phys. Rev. Lett.* **2009**, *103*, 053602. [CrossRef] [PubMed]
7. Hao, J.; Liu, T.; Huang, Y.; Chen, G.; Liu, A.; Wang, S.; Wen, W. Metal nanoparticle-nanowire assisted SERS on film. *J. Phys. Chem. C* **2015**, *119*, 19376–19381. [CrossRef]
8. Wu, T.; Liu, Y.; Yu, Z.; Ye, H.; Peng, Y.; Shu, C.; Yang, C.; Zhang, W.; He, H. A nanometeric temperature sensor based on plasmonic waveguide with an ethanol-sealed rectangular cavity. *Opt. Commun.* **2015**, *339*, 1–6. [CrossRef]
9. Kashif, M.; Bakar, A.A.; Arsad, N.; Shaari, S. Development of phase detection schemes based on surface plasmon resonance using interferometry. *Sensors* **2014**, *14*, 15914–15938. [CrossRef] [PubMed]
10. Brolo, A.G. Plasmonics for future biosensors. *Nat. Photonics* **2012**, *6*, 709–713. [CrossRef]

11. Jiang, Y.; Wang, H.Y.; Wang, H.; Gao, B.R.; Hao, Y.W.; Jin, Y.; Chen, Q.D.; Sun, H.B. Surface plasmon enhanced fluorescence of dye molecules on metal grating films. *J. Phys. Chem. C* **2011**, *115*, 12636–12642. [CrossRef]
12. Fang, Y.; Sun, M. Nanoplasmonic waveguides: Towards applications in integrated nanophotonic circuits. *Light Sci. Appl.* **2015**, *4*, e294. [CrossRef]
13. Chen, Z.; Yu, L. Multiple fano resonances based on different waveguide modes in a symmetry breaking plasmonic system. *IEEE Photonics J.* **2014**, *6*, 1–8. [CrossRef]
14. Tong, L.M.; Wei, H.; Zhang, S.P.; Xu, H.X. Recent advances in plasmonic sensors. *Sensors* **2014**, *14*, 7959–7973. [CrossRef] [PubMed]
15. Zhang, Z.; Wang, J.; Zhao, Y.; Lu, D.; Xiong, Z. Numerical investigation of a branch-shaped filter based on metal-insulator-metal waveguide. *Plasmonics* **2011**, *6*, 773–778. [CrossRef]
16. Wu, Y.D. High transmission efficiency wavelength division multiplexer based on metal-insulator-metal plasmonic waveguides. *J. Lightwave Technol.* **2014**, *32*, 4844–4848.
17. Xie, Y.Y.; Huang, Y.X.; Zhao, W.L.; Xu, W.H.; He, C.A. Novel Plasmonic sensor based on metal-insulator-metal waveguide with side-coupled hexagonal cavity. *IEEE Photonics J.* **2015**, *7*, 1–12. [CrossRef]
18. Qi, J.; Chen, Z.; Chen, J.; Li, Y.; Qiang, W.; Xu, J.; Sun, Q. Independently tunable double Fano resonances in asymmetric MIM waveguide structure. *Opt. Express* **2014**, *22*, 14688–14695. [CrossRef] [PubMed]
19. Lee, K.L.; Huang, J.B.; Chang, J.W.; Wu, S.H.; Wei, P.K. Ultrasensitive biosensors using enhanced Fano resonances in capped gold nanoslit arrays. *Sci. Rep.* **2015**, *5*, 08547–08555. [CrossRef] [PubMed]
20. Chen, J.; Sun, C.; Gong, Q. Fano resonances in a single defect nanocavity coupled with a plasmonic waveguide. *Opt. Lett.* **2014**, *39*, 52–55. [CrossRef] [PubMed]
21. Chen, J.; Li, Z.; Zou, Y.; Deng, Z.; Xiao, J.; Gong, Q. Coupled-resonator-induced Fano resonances for plasmonic sensing with ultra-high figure of merits. *Plasmonics* **2013**, *8*, 1627–1631. [CrossRef]
22. Luk'yanchuk, B.; Zheludev, N.I.S.; Maier, A.; Halas, N.J.; Nordlander, P.; Giessen, H.; Chong, T.C. The Fano resonance in plasmonic nanostructures and metamaterials. *Nat. Mater.* **2010**, *9*, 707–715. [CrossRef] [PubMed]
23. Rahmani, M.; Luk'yanchuk, B.; Hong, M. Fano resonance in novel plasmonic nanostructures. *Laser Photonics Rev.* **2013**, *7*, 329–349. [CrossRef]
24. Miroshnichenko, A.E.; Flach, S.; Kivshar, Y.S. Fano resonances in nanoscale structures. *Rev. Mod. Phys.* **2010**, *82*, 2257–2298. [CrossRef]
25. Wu, T.; Liu, Y.; Yu, Z.; Peng, Y.; Shu, C.; Ye, H. The sensing characteristics of plasmonic waveguide with a ring resonator. *Opt. Express* **2014**, *22*, 7669–7677. [CrossRef] [PubMed]
26. Yan, S.B.; Luo, L.; Xue, C.Y.; Zhang, Z.D. A refractive index sensor based on a metal-insulator-metal waveguide-coupled ring resonator. *Sensors* **2015**, *15*, 29183–29191. [CrossRef] [PubMed]
27. Xie, Y.Y.; Huang, Y.X.; Che, H.J.; Zhao, W.L.; Xu, W.H.; Li, X.; Li, J. Theoretical investigation of a plasmonic sensor based on a metal-insulator-metal waveguide with a side-coupled nanodisk resonator. *J. Nanophotonics* **2015**, *9*, 093099-1–093099-13. [CrossRef]
28. Chen, Z.; Wang, W.; Cui, L.; Yu, L.; Duan, G.; Zhao, Y.; Xiao, J. Spectral splitting based on electromagnetically induced transparency in plasmonic waveguide resonator system. *Plasmonics* **2014**, *10*, 721–727. [CrossRef]
29. Chen, Z.; Song, X.; Jiao, R.; Duan, G.; Wang, L.; Yu, L. Tunable electromagnetically induced transparency in plasmonic system and its application in nanosensor and spectral splitting. *IEEE Photonics J.* **2015**, *7*, 4801408-1–4801408-8.
30. Zhang, S.; Bao, K.; Halas, N.J.; Xu, H.; Nordlander, P. Substrate-induced Fano resonances of a plasmonic nanocube: A route to increased-sensitivity localized surface plasmon resonance sensors revealed. *Nano Lett.* **2011**, *11*, 1657–1663. [CrossRef] [PubMed]
31. Hayashi, S.; Nesterenko, D.V.; Sekkat, Z. Waveguide-coupled surface plasmon resonance sensor structures: Fano lineshape engineering for ultrahigh-resolution sensing. *J. Phys. D Appl. Phys.* **2015**, *48*, 325303. [CrossRef]
32. Kekatpure, R.D.; Hryciw, A.C.; Barnard, E.S.; Brongersma, M.L. Solving dielectric and plasmonic waveguide dispersion relations on a pocket calculator. *Opt. Express* **2009**, *17*, 24112–24129. [CrossRef] [PubMed]
33. Gai, H.; Wang, J.; Tian, Q. Modified Debye model parameters of metals applicable for broadband calculations. *Appl. Opt.* **2007**, *46*, 2229–2233. [CrossRef] [PubMed]
34. Zhu, J.H.; Wang, Q.J.; Shum, P.; Huang, X.G. A simple nanometeric plasmonic narrow-band filter structure based on metal-insulator-metal waveguide. *IEEE Trans. Nanotechnol.* **2011**, *10*, 1371–1376. [CrossRef]

35. Hu, F.; Yi, H.; Zhou, Z. Wavelength demultiplexing structure based on arrayed plasmonic slot cavities. *Opt. Lett.* **2011**, *36*, 1500–1502. [CrossRef] [PubMed]
36. Haus, H.A. *Waves and Fields in Optoelectronics*; Prentice-Hall: Upper Saddle River, NJ, USA, 1984.
37. Haus, H.A.; Huang, W.P. Coupled-mode theory. *IEEE Proc.* **1991**, *79*, 1505–1518. [CrossRef]
38. Piao, X.; Yu, S.; Koo, S.; Lee, K.; Park, N. Fano-type spectral asymmetry and its control for plasmonic metal-insulator-metal stub structures. *Opt. Express* **2011**, *19*, 10907–10912. [CrossRef] [PubMed]
39. Roh, S.; Chung, T.; Lee, B. Overview of the characteristics of micro- and nano-structured surface plasmon resonance sensors. *Sensors* **2011**, *11*, 1565–1588. [CrossRef] [PubMed]